Anthropogenic influences on the physical state of submicron particulate matter over a tropical forest

Adam P. Bateman[1], Zhaoheng Gong[1], Tristan H. Harder[2], Suzane S. de Sá[1], Bingbing Wang[3,4], Paulo Castillo[5], Swarup China[3], Yingjun Liu[1], Rachel E. O'Brien[2,6], Brett Palm[7], Hung-Wei Shiu[3], Glauber da Silva[8], Ryan Thalman[5], Kouji Adachi[9], M. Lizabeth Alexander[3], Paulo Artaxo[10], Allan K. Bertram[11], Peter R. Buseck[12], Mary K. Gilles[2], Jose L. Jimenez[7], Alexander Laskin[3], Antonio O. Manzi[8], Arthur Sedlacek[5], Rodrigo A. F. Souza[13], Jian Wang[5], Rahul Zaveri, Scot T. Martin[*1,14]

[1]School of Engineering and Applied Sciences, Harvard University, Cambridge, Massachusetts, USA
[2]Chemical Sciences Division, Lawrence Berkeley National Laboratory, Berkeley, CA, USA
[3]William R. Wiley Environmental Molecular Sciences Laboratory, Pacific Northwest National Laboratory, Richland, WA, USA
[4]State Key Laboratory of Marine Environmental Science, College of Ocean and Earth Sciences, Xiamen University, Xiamen, China
[5]Brookhaven National Laboratory, Upton, New York, USA
[6]Department of Civil and Environmental Engineering, Massachusetts Institute of Technology, Cambridge, Massachusetts, USA
[7]University of Colorado, Boulder, USA
[8]National Institute of Amazonian Research, Amazonas, Brazil
[9]Atmospheric Environment and Applied Meteorology Research Department, Meteorological Research Institute, Tsukuba, Ibaraki, Japan
[10]University of São Paulo, São Paulo, Brazil
[11]Department of Chemistry, University of British Columbia, Vancouver, BC, Canada
[12]School of Earth and Space Exploration & School of Molecular Sciences, Arizona State University, Tempe, Arizona, USA
[13]Amazonas State University, Amazonas, Brazil
[14]Department of Earth and Planetary Sciences, Harvard University, Cambridge, Massachusetts, USA

Atmospheric Chemistry and Physics

[*] Correspondence to: S.T. Martin (scot_martin@harvard.edu)

Supplement

S1. Impactor protocols

A rebound curve representing *f*(RH) constituted an individual data set, where *f* is the rebound fraction of Equation 1. The DMA setting for electric mobility was held constant, the RH in the humidification unit was scanned stepwise, and *f* was continuously recorded. During the course of measurements, rebound curves were collected by several protocols. During IOP1, these protocols included: (1) constant RH while increasing the mobility diameter in variable steps every 3 min from 50 to 190 nm, resulting in a full sweep in 30 min; (2) constant RH while shifting mobility diameter among 120, 150, and 190 nm every 16 min; and (3) fixed mobility diameter at 190 nm while increasing the RH stepwise every 5 to 10 min. For each of these three protocols, 8 to 11 RH levels were probed to produce a rebound curve. The data in the main text correspond to the third protocol, and a rebound curve was collected in 40 to 90 min. Some of the supplementary figures represent data collected with the other two protocols. For IOP2, improved computer control over the apparatus allowed more efficient protocols to be used: (1) constant RH while shifting mobility diameters among 150, 190, and 240 nm every 3 to 5 min and (2) fixed mobility diameter at 190 nm while increasing RH stepwise every 3 to 5 min. RH levels were also controlled at a finer scale, and a rebound curve consisted of 20 RH settings. The data in the main text correspond to the second protocol, and a rebound curve was collected in 30 to 60 min.

S2. Microscopy Description

An X-ray beam obtained at soft wavelengths from the synchrotron light source was used to probe chemical bonding of specific elements of interest within individual particles. Carbon and oxygen K-edge NEXAFS spectra were acquired in this study. Mixing state and chemical bonding of elements within individual particles at a size resolution of 35 nm were identified by

analyzing the recorded spectra. A set ("stack") of STXM images was obtained by raster scanning the sample at fixed photon energy and recording intensities of the transmitted X-rays at each pixel. The spatially resolved NEXAFS spectra were retrieved for the specific areas of interest from the recorded STXM stacks.

S3. Determining rebound fraction at ambient RH

The ambient RH was monitored continuously during the GoAmazon2014/5 campaign. Data were obtained at one-minute intervals by the ARM Mobile Facility One (AMF-1). Rebound fractions were associated with ambient RH values which matched the apparatus (inlet) RH bins within 15 min of measurement. Nine bins were used for IOP1 with RH values of 0, 58, 63, 68, 73, 78, 83, 88, 93, and 100%. Twenty-two bins were used for IOP2 with RH values of 0, 35, 40, 45, 50, 55, 60, 62.5, 65, 67.5, 70, 72.5, 75, 77.5, 80, 82.5, 85, 87.5, 90, 92.5, 97.5, and 100%.

The results of the binning method are shown in Figure S3. The rebound fraction is displayed versus the apparatus (inlet) relative humidity for (a) IOP1 and (d) IOP2 and versus the ambient relative humidity for (b) IOP1 and (e) IOP2. An evaluation of the RH binning procedure can be seen in (c) IOP1 and (f) IOP2, which display the apparatus RH versus the ambient RH. The coefficients R^2 of determination for the linear fits in (c) and (f) are listed in Table S5. The range seen in ambient values obtained from each inlet RH bin arises from the 15-min intervals used to match apparatus RH and ambient RH values. The multiple values for apparatus (inlet) RH obtained from the lowest ambient RH values are due to the large bin used, i.e., 0 to 58 % RH and 0 to 35 % RH for IOP1 and IOP2, respectively.

S4. Air-Mass Classification

Two separate air mass classification schemes were used in conjunction to determine the predominant conditions at the T3 site. The first classification scheme was used primarily to

identify time periods when the T3 site was influenced by anthropogenic pollution from Manaus (Cirino et al., 2016). In the cited study, particle number and CO concentrations were used to indicate the presence of Manaus plume. Herein, the 25% and 75% quantiles were used to define the thresholds for the T3 site according to the bounds listed in Table S6. Background conditions were indicated when concentrations were below the thresholds listed in Table S6. Observations at a remote forest site T0a were used to establish the thresholds (Thalman, 2016). The established thresholds were different depending on the dry or wet season. Biomass burning conditions were determined by the threshold number of particles and the number fraction of particles below 70 nm. The threshold value for the number fraction is indicated in Table S6 (Thalman, 2016). The periods not resolved (i.e., "unclassified") includes cases of (i) unavailable from the monitoring instruments (e.g., maintenance or repair) and (ii) all simultaneous criteria needed for positive classification were not met. The number and fraction of data points classified into the four categories are listed in Table S7.

S5. Deviations relative to background conditions calculation

The deviations relative to background conditions represent the contribution to the rebound fraction above the background-average rebound response curve. The reference curve is based on data sets for which the rebound fraction was less than 0.05 at an apparatus RH of 80%. The reference curves for IOP1 and IOP2 are plotted in the left and right panels of Figure S4, respectively. In each panel, the black line is the reference curve, and the red lines represent upper and lower bounds, respectively, based on one-sigma error propagation of the CPC measurements. The green points are within the envelope of the reference curves determined for IOP1 and IOP2.

For all data points, the deviation Δf relative to the reference curve was calculated as follows:

$$\begin{aligned} &\text{For } f(RH) < f_{\text{upper,reference}}, \Delta f(RH) = f(RH) - f_{\text{upper,reference}}(RH). \\ &\text{Otherwise, } \Delta f(RH) = 0. \end{aligned} \quad \text{(S1)}$$

The spread in rebound fractions for RH < 50% is investigated in Figure S5a. The rebound fractions from a variety of materials are plotted as a function of RH, including chamber PM, Amazonia PM measured during 2013, and particles of sucrose, citric acid, and ammonium sulfate. The reference curves from IOP1 and IOP2 are plotted for comparison. The measured rebound fractions ranged from 0.8 to 1.1 for the investigated materials. Even though there are differences in physical state (e.g., crystalline, amphorous solid, and so on) for the investigated materials, there is no systematic trend for RH < 50% that can be associated with the known physical states and thus applied as a rubric to the scatter observed from the field data. The large spread in measured rebound fractions at RH < 50% observed during IOP1 and IOP2 cannot then be used to distinguish a potential distribution of particle viscosities.

The spread in measured rebound fractions for RH > 50% is investigated in Figure S5b. The same set of test compounds are used as in Figure S5a. The rebound response curves of the organic test materials exhibit shifts at RH values according to their relative hygroscopicity. Particle rebound greater in excess of the reference curve (i.e., rebound deviation) can therefore be used as a proxy for semisolidity for RH > 50%.

S6. AMS PMF Factors

Six positive matrix factorization (PMF) factors explained the variance in the AMS datasets during IOP1 and IOP2. Labeled as factors “1” through “6”, these factors traditionally have been associated with the processes/classes of (1) IEPOX-derived secondary organic species (IEPOX-SOA), (2) more-oxidized (i.e., “aged”) secondary organic species (MO-OOA), (3) less-

oxidized (i.e., “fresher”) secondary organic species (LO-OOA), (4) more-oxidized biomass burning compounds (MO-BBOA), (5) less-oxidized biomass burning compounds (LO-BBOA) for IOP2 and a factor currently hypothesized to be representative of organic material derived from aromatic compounds for IOP1, and (6) hydrocarbon-like organic compounds from unburned primary emissions released by fuel combustion (HOA) (de Sá, 2016). The PMF factors obtained for each season were for the most part similar, except for factor 5. For IOP2, factor 5 reflected the increase in local and regional biomass burning in the dry season, which allowed for a separation of a second BBOA factor, while for IOP1 it reflected the influence of urban pollution reaching T3 in the absence of extensive biomass burning (de Sá, 2016).

In the present study, the loadings of PMF factors 1, 2 and 3, and PMF factors 4, 5, and 6 were separately lumped. The respective groupings are referred to as PMF group A and PMF group B. PMF group A represents the influence of background processes while PMF group B represents the influences of urban pollution and biomass burning processes.

S7. Probability density function of rebound deviation segregated by air mass type

The distribution of rebound deviations relative to background conditions for each classification and IOP are listed in Table S2. Deviations relative to background conditions of greater than +0.1 represented 17% of the total observations during IOP1. Deviations of greater than +0.1 represented 35% of the total observations for IOP2. The increase in the frequency of large deviations relative to background conditions during IOP2 compared to IOP1 is explained by the influence of biomass burning.

S8. κ_G Determination for subsaturated conditions

The analysis for determing κ_G was published previously (Bateman et al., 2016). A brief description is provided herein. The transmission functions $\Omega_{uncoated}$ and Ω_{coated} for the uncoated and coated arms, respectively, were calculated as follows:

$$\Omega_{\text{uncoated}} = \frac{N_{\text{i}}}{N_{\text{iii}}},\ \Omega_{\text{coated}} = \frac{N_{\text{ii}}}{N_{\text{iii}}} \tag{S2}$$

from transmitted particle number concentrations N measured by the three condensation particle counters. The sigmoid function representing the transmission function was used to fit the setpoint mobility diameter d_m^* and a width parameter δ.

$$\Omega(d_m) = \frac{1}{1+\exp\left(\left(d_m - d_m^*\right)/\delta\right)} \tag{S3}$$

The fit value of d_m^* was converted to a setpoint aerodynamic diameter d_a^* according to:

$$d_a = \left(\frac{\rho_p}{\rho_0}\frac{C_c(d_m)}{C_c(d_a)}\right)^{1/2} d_m \tag{S4}$$

This equation is for a limiting assumption of nonporous spherical particles having +1 charge (Kelly and McMurry, 1992). Terms include the particle material density ρ_p, a reference material density ρ_0 (1000 kg m^{-3}), and the Cunningham slip correction factors $C_c(d_m)$ and $C_c(d_a)$.

Of key interest for determing κ_G, the material density $\rho_{p,i}$ of the different data sets i depended on relative humidity. The density was assumed to follow a volume mixing rule between $\rho_{p,\text{dry}}$ of the organic material and $\rho_{p,\text{water}}$ of water (Brechtel and Kreidenweis, 2000). The fractional particle water volume was derived by assuming the following relationship:

$$G = \left[1+\left(\frac{\text{RH}/100}{\text{1-RH}/100}\right)\kappa\right]^{1/3} \tag{S5}$$

In this equation, G is the diameter-based hygroscopic growth factor, RH is relative humidity, and κ is the hygroscopicity parameter. Values of $\rho_{p,\mathrm{dry}}$ and κ, as needed to estimate $\rho_{p,i}$ of each experiment, were obtained by optimization of four datasets. The minimized quantity was $\sum_i \left(d^*_{a,i} - d^*_{a,0}\right)^2$ for each dataset for which $d^*_{a,0}$ = 84.9 nm. For each i, $d^*_{a,i}$ was obtained using Equation S4 with parameter values of $d^*_{m,i}$ and $\rho_{p,i}(\rho_{p,\mathrm{dry}},\kappa)$ obtained by the volume mixing rule. Values of $\rho_{p,\mathrm{dry}}$ and κ were taken as constant within each RH-dependent dataset. The values of κ were then averaged over the four successive datasets to obtain the values used in the Figure 7.

The measured κ_G during IOP1 can be compared with literature values from hygroscopic tandem differential mobility analyzer (H-TDMA) instruments. The results from several studies in Amazonia are compiled in Table S3. There are several important distinctions to note between the H-TDMA measurements and the measurements of κ_G by the impactor apparatus. Particle rebound ceases for $G > 1.10 \pm 0.02$ corresponding to a κ_G of 0.06 at 90% RH. The impactor apparatus while being operated at 90% RH is then able to distinguish particles with κ_G of less than 0.06 from those with κ_G greater than 0.06. The measured value is thus a lower limit of the actual value because any particle having $\kappa_G > 0.06$ ($f = 0$) cannot be distinguished from particles of greater κ_G. Particles of differing κ_G can be distinguished as a function of RH as in the impactor apparatus. Therefore, in the analysis κ_G values are evaluated for datasets obtained at multiple RH values and averaged to obtain a global κ_G.

S9. Modeled compared to measured rebound deviation

Rebound deviation was predicted according to the following equation:

$$\Delta f_{predicted}(\mathrm{RH}) = \mathrm{PMF\text{-}A} \cdot x_1 + \mathrm{PMF\text{-}B} \cdot x_2 \qquad \text{(S6)}$$

where PMF-A and PMF-B are the fractional loadings of PMF groups A and x_1 and x_2 are linear coefficients. The coefficients were obtained by optimization of each dataset as a function of RH.

The minimized quantity was $\sum_i \left(\Delta f(\mathrm{RH})_{predicted,i} - \Delta f(\mathrm{RH})_{measured} \right)^2$ for each season and RH range.

The RH ranges are listed in Table S4 along with the optimized coefficients.

Table S1. Percent of data points when grouped into steps of 0.05 rebound fraction. "All Data" refers to measurements collected at all apparatus RH values. "Ambient RH" refers to measurements collected when the apparatus RH matched the ambient RH value (cf. Supplement S3). Cumulative values are represented in parentheses.

Rebound Deviation	All Data		Ambient RH	
	IOP1	IOP2	IOP1	IOP2
< 0.05	71.3% (71.3%)	50.4% (33.9%)	44.9% (44.9%)	53.8% (53.8%)
0.05 – 0.10	12.2% (83.5%)	14.8% (65.2%)	34.7% (79.5%)	22.6% (76.4%)
0.10 – 0.20	11.2% (94.7%)	18.4% (83.6%)	16.5% (96.0%)	17.6% (94.0%)
0.20 – 0.30	4.1% (98.8%)	9.8% (93.4%)	3.3% (99.3%)	4.7% (98.7%)
0.30 – 0.40	1.1% (99.9%)	5.5% (98.9%)	0.7% (100%)	1.3% (100.0%)
> 0.40	<0.1% (100%)	1.1% (100%)	0.0 % (100%)	0.0% (100%)

Table S2. Percent of all data points when grouped into steps of 0.05 rebound fraction according to type of air mass. Cumulative values are represented in parentheses.

	Background Conditions		Manaus Pollution		Biomass Burning		Unclassified	
Rebound Deviation	**IOP1**	**IOP2**	**IOP1**	**IOP2**	**IOP1**	**IOP2**	**IOP1**	**IOP2**
< 0.05	81.3% (81.3%)	80.6% (80.6%)	51.7% (51.7%)	66.8% (66.8%)	-	42.8% (42.8%)	65.4% (65.4%)	57.9% (57.9%)
0.05 – 0.10	7.9% (89.2%)	9.0% (89.6%)	14.0% (65.7%)	14.9% (81.7%)	-	15.6% (58.4%)	18.8% (84.2%)	14.9% (72.8%)
0.10 – 0.20	8.6% (97.8%)	7.0% (96.6%)	17.2% (82.9%)	12.9% (94.6%)	-	21.2% (79.6%)	12.6% (96.8%)	16.0% (88.8%)
0.20 – 0.30	1.5% (99.3%)	3.1% (99.7%)	12.5% (95.4%)	4.6% (99.2%)	-	11.9% (91.5%)	2.8% (99.6%)	6.6% (95.4%)
0.30 – 0.40	0.7% (100%)	0.3% (100%)	4.3% (99.7%)	0.7% (99.9%)	-	7.1% (98.6%)	0.4% (100%)	4.0% (99.4%)
> 0.40	0.0% (100%)	0.0% (100%)	0.3% (100%)	0.1% (100%)	-	1.5% (100%)	0.0% 100%)	0.7% (100%)

Table S3. Comparison of κ_G values of hydrophobic and hygroscopic fraction of particles using H-TDMA measurements (literature) with the values obtained from the impactor apparatus (current study). Population fractions correspond to dry diameters of 190 nm for IOP1 and both 190 and 240 nm for IOP2. Growth factor data from IOP1 and the study of 2013 reported in Bateman et al. (2016) are associated with dry particle diameters of 50 to 70 nm.

[see table next page]

Particle Population Distribution	Wet Season				Transition Season				Dry Season		
	IOP1 – All Data	2013	†LBA – SMOCC -2002	†CLAIRE – 98	†LBA – SMOCC - 2002	†CLAIRE – 2001 Clean	†CLAIRE – 2001 Recent BB	†CLAIRE – 2001 Aged BB	IOP2 – All Data	2013	†LBA – SMOCC-2002
Hydrophobic Particles											
Frequency of Occurrence	56.5%	-	89 - 92 %	14 - 11 %	96 - 97 %	26% - 49 %	58 - 76%	21 - 79%	39.4%	-	99 - 99%
Number Fraction (when present)	0.095 ± 0.060	-	0.40 - 0.34 ±0.21	0.31 - 0.24 ± 0.19	0.62 - 0.42 ±0.26	0.14 - 0.28 ±0.11	0.19 - 0.23 ±0.12	0.18 -0.34 ±0.17	0.100 ± 0.069	-	0.84 - 0.69 ±0.29
κ	0.041	-	0.040 -0.047	0.003 - 0.010*	0.036 - 0.043	0.018 - 0.058*	0.045 - 0.045*	0.049 - 0.058*	-	-	0.037 -0.044
Hygroscopic Particles											
Frequency of Occurrence	100%	-	99 - 100 %	95 - 97 %	86 - 96 %	100 - 100%	100%	100 - 100%	100%	-	51 - 66 %
Number Fraction (when present)	0.937 ± 0.066	-	0.66 - 0.69 ±0.23	0.94 - 0.97 ± 0.15	0.47 - 0.62 ±0.24	0.96 - 0.86 ± 0.17	0.88 - 0.83 ±0.14	0.96 - 0.73 ±0.21	0.958 ± 0.067	-	0.32 - 0.48 ±0.22
κ	0.090	-	0.124 - 0.146	0.111 -0.144*	0.113 -0.123	0.122 -0.150*	0.150 - 0.168*	0.139 - 0.162*	-	-	0.111 - 0.113
κ, both modes‡	0.09	0.053	0.124-0.128	0.096-0.115‡	0.106-0.112	0.108-0.118‡	0.117-0.122‡	0.116-0.116‡	-	0.063	0.079-0.094

*****Values of κ were not reported in the original manuscript and have been calculated according to Equation S5 using the reported G values.

†Range of values is for particles of 165 nm and 265 nm

‡Average values of κ for both modes are calculated assuming volume additivity.

Table S4. The optimized coefficients used to predict rebound deviation (Equation S6).

IOP1	PMF Group A	PMF Group B
	x_1	x_2
48 – 53% RH	0.00	0.00
53 – 63% RH	0.00	0.00
63 – 68% RH	0.00	0.06
68 – 73% RH	0.00	0.27
73 – 78% RH	0.00	0.33
78 – 83% RH	0.00	0.30
83 – 88% RH	0.00	0.33
88 – 93% RH	0.00	0.32
> 93% RH	0.00	0.25

IOP2	PMF Group A	PMF Group B
	x_1	x_2
48 – 53% RH	0.00	0.00
53 – 63% RH	0.01	0.16
63 – 68% RH	0.03	0.39
68 – 73% RH	0.04	0.51
73 – 78% RH	0.04	0.55
78 – 83% RH	0.00	0.51
83 – 88% RH	0.00	0.37
88 – 93% RH	0.00	0.24
> 93% RH	0.00	0.14

Table S5. Statistics on the binning method used to predict the rebound fraction at ambient RH from the measurements of rebound fraction at specific apparatus RH values (cf. Figure S3).

	Apparatus RH Bin Method	
	IOP1	IOP2
Number of Matched Data Points	308 (8%)	3055 (11%)
Coefficient R^2 of Determination Between Apparatus and Ambient RH	0.94	0.95

Table S6. Parameters and bounds used to classify the air masses passing over the T3 site. Classifications include background, pollution, or biomass burning. Time periods that did not fit these bounds are labeled unclassified. The parameters included the particle number concentrations (CN), ratio of the latter to ΔCO (where ΔCO was the difference in CO measured at the T3 site and the T2 site to account for dilution), the concentration of gas-phase NO_y, and the fraction (CN_{frac}) of particles smaller 70 nm.

Classification	Wet Season (IOP1)	Dry Season (IOP2)
Background	40 cm^{-3} ppbv > CN/ΔCO CN < 500 cm^{-3} CO < 140 ppbv NO_y < 0.9 ppbv	40 cm^{-3} ppbv > CN/ΔCO CN < 1500 cm^{-3} NO_y < 1.5 ppbv
Pollution	40 < CN/ΔCO <130 cm^{-3} ppbv	40 < CN/ΔCO <130 cm^{-3} ppbv
Biomass Burning	CN > 500 cm^{-3} CN_{frac} < 0.45	CN>1500 cm^{-3} CN_{frac} < 0.45

Table S7. The frequency of occurrence for each classification along with the total number of data points in that classification.

	Background Conditions		Manaus Pollution		Biomass Burning		Unclassified	
	IOP1	**IOP2**	**IOP1**	**IOP2**	**IOP1**	**IOP2**	**IOP1**	**IOP2**
Frequency	17%	10%	24%	11%	-	71%	58%	8%
Number of Points	278	911	400	955	-	6377	972	717

Table S8. Time series of data.

[See electronic attachment to the PDF file]

Figure Captions

Figure S1. Scatter plot of rebound deviation with meteorological measurements at the T3 site. Correlations with ambient temperature, wind direction, and wind speed are shown for (a) IOP1 daytime, (b) IOP1 nighttime, (c) IOP2 daytime, and (d) IOP2 nighttime. Median values for four bins having equal numbers of data points are indicated by black circles. Whiskers represent quartile values. Relative humidity is variable throughout the data points in the panels, corresponding to all data points shown in Figure 1a.

Figure S2. Scatter plot of rebound deviation with auxiliary particle measurements at the T3 site. Correlations with submicron particle mass concentration, black carbon concentration, and sulfate concentration are shown for (a) IOP1 daytime, (b) IOP1 nighttime, (c) IOP2 daytime, and (d) IOP2 nighttime. Median values for four bins having equal numbers of data points are indicated by black circles. Whiskers represent quartile values.

Figure S3. Rebound fraction and relative humidity after co-binning. The top and bottom panels are associated with IOP1 and IOP2, respectively. The first column (panels a and d) displays the rebound fraction as a function of the apparatus (inlet) relative humidity. The middle column (panels b and e) displays the rebound fraction as a function of the ambient relative humidity. The last column (panels c and f) displays the apparatus (inlet) relative humidity versus the ambient relative humidity (cf. Table S5).

Figure S4. Rebound fractions measured during (a) IOP1 and (b) IOP2 compared to the background-average reference curve (black lines) and its upper and lower bounds

(red lines) (cf. Section S4 of the Supplement). Results are shown for particles having a mobility diameter of 190 nm. The RH values correspond to those inside the impactor.

Figure S5. Rebound curves for a variety of test materials including chamber PM, Amazonia PM measured during 2013, and particles of sucrose, citric acid, and ammonium sulfate. (a) Rebound fractions for < 50% RH. (b) Rebound fractions for > 50% RH. The shaded regions show the full range of rebound fractions measured during IOP1 and IOP2. The background-average values are also plotted for reference.

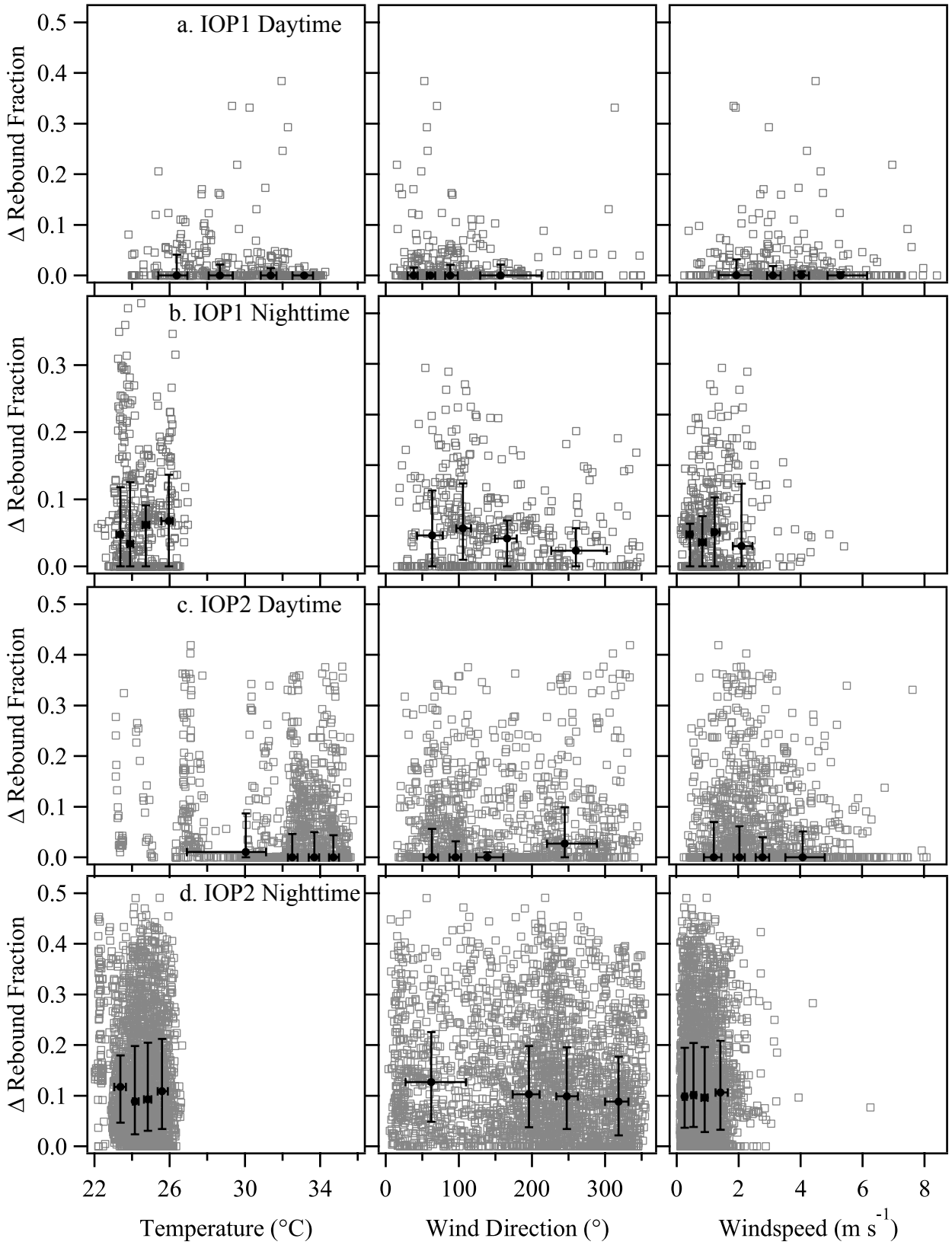
a. IOP1 Daytime
b. IOP1 Nighttime
c. IOP2 Daytime
d. IOP2 Nighttime
Δ Rebound Fraction
0.0
0.1
0.2
0.3
0.4
0.5
22
26
30
34
0
100
200
300
0
2
4
6
8
Temperature (°C)
Wind Direction (°)
Windspeed (m s-1)

Figure S1

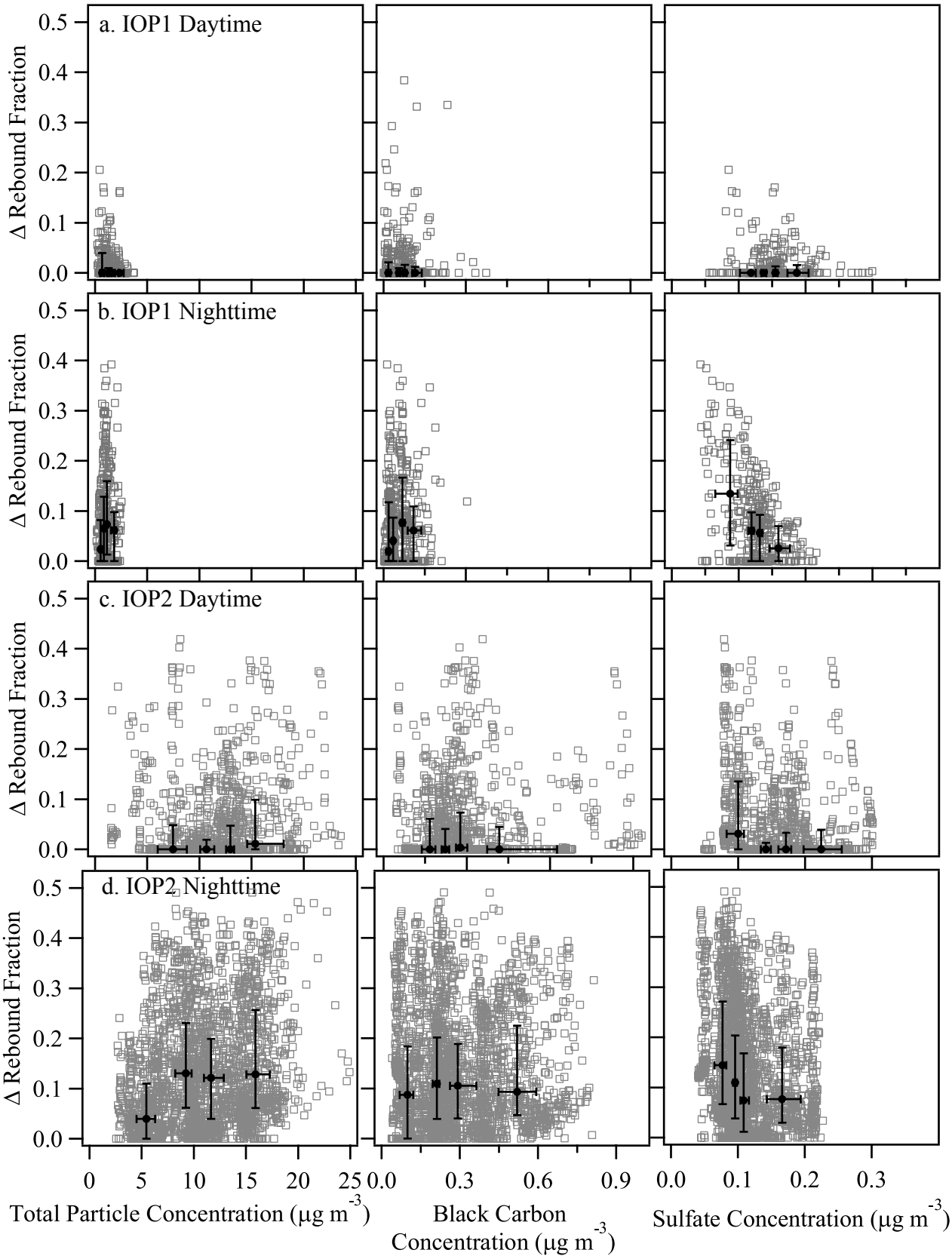
a. IOP1 Daytime
b. IOP1 Nighttime
c. IOP2 Daytime
d. IOP2 Nighttime
Δ Rebound Fraction
0.0
0.1
0.2
0.3
0.4
0.5
0
5
10
15
20
25
0.0
0.3
0.6
0.9
0.0
0.1
0.2
0.3
Total Particle Concentration (μg m-3)
Black Carbon Concentration (μg m-3)
Sulfate Concentration (μg m-3)

Figure S2

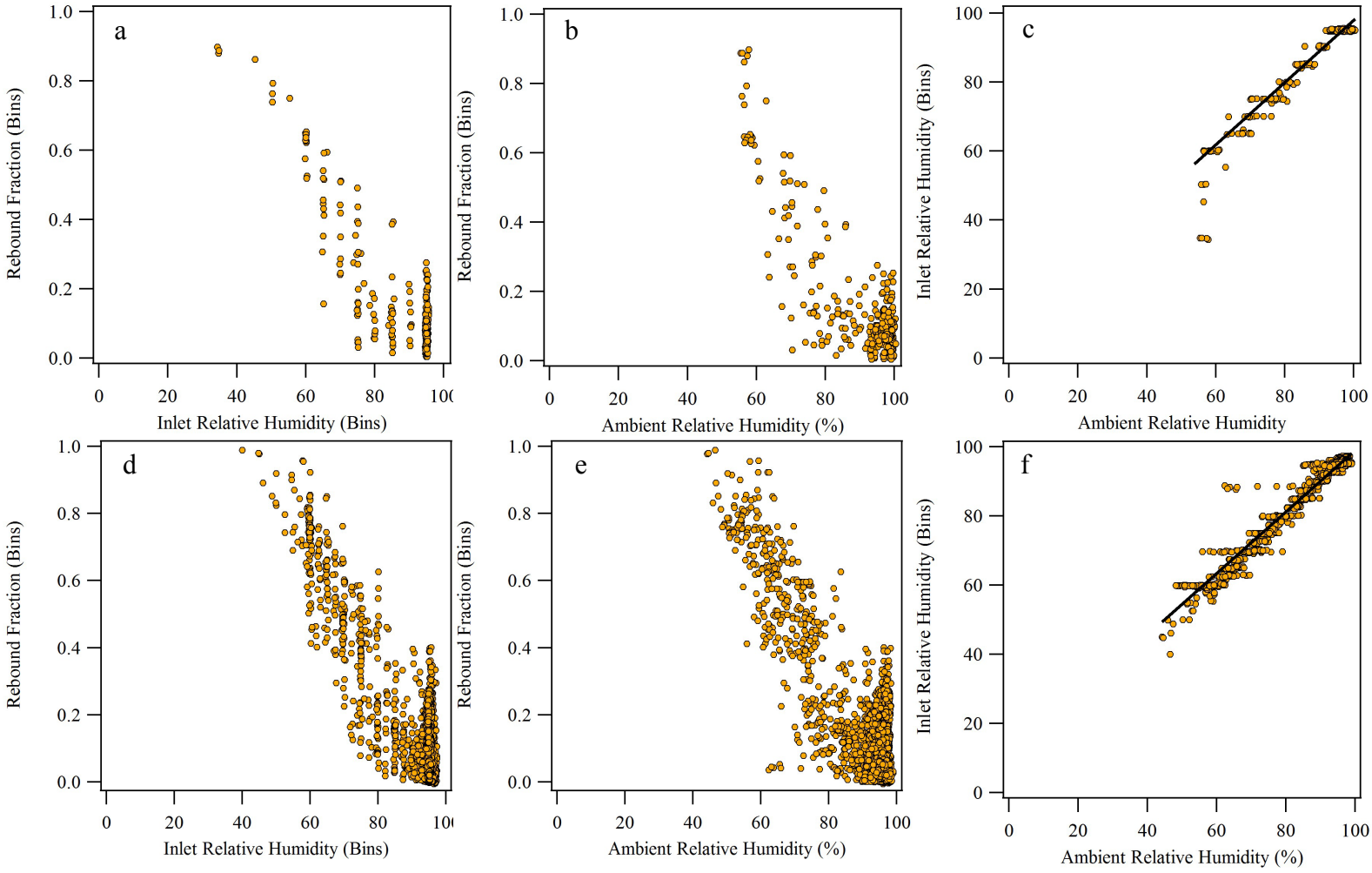
a
b
c
d
e
f
Rebound Fraction (Bins)
Inlet Relative Humidity (Bins)
Ambient Relative Humidity (%)
Inlet Relative Humidity (Bins)
Ambient Relative Humidity
Ambient Relative Humidity (%)

Figure S3

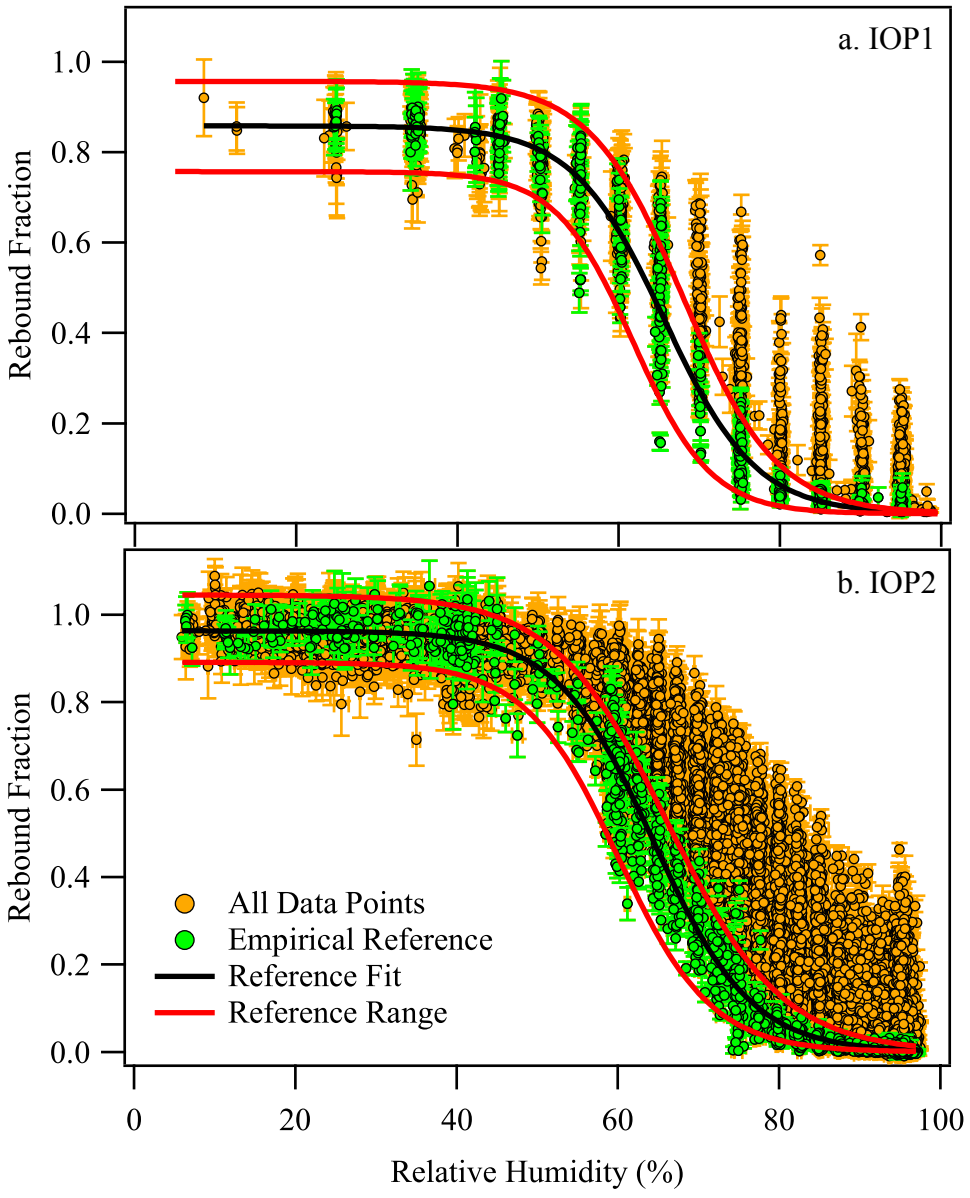
a. IOP1
b. IOP2
Rebound Fraction
Relative Humidity (%)
All Data Points
Empirical Reference
Reference Fit
Reference Range
0.0
0.2
0.4
0.6
0.8
1.0
0
20
40
60
80
100

Figure S4

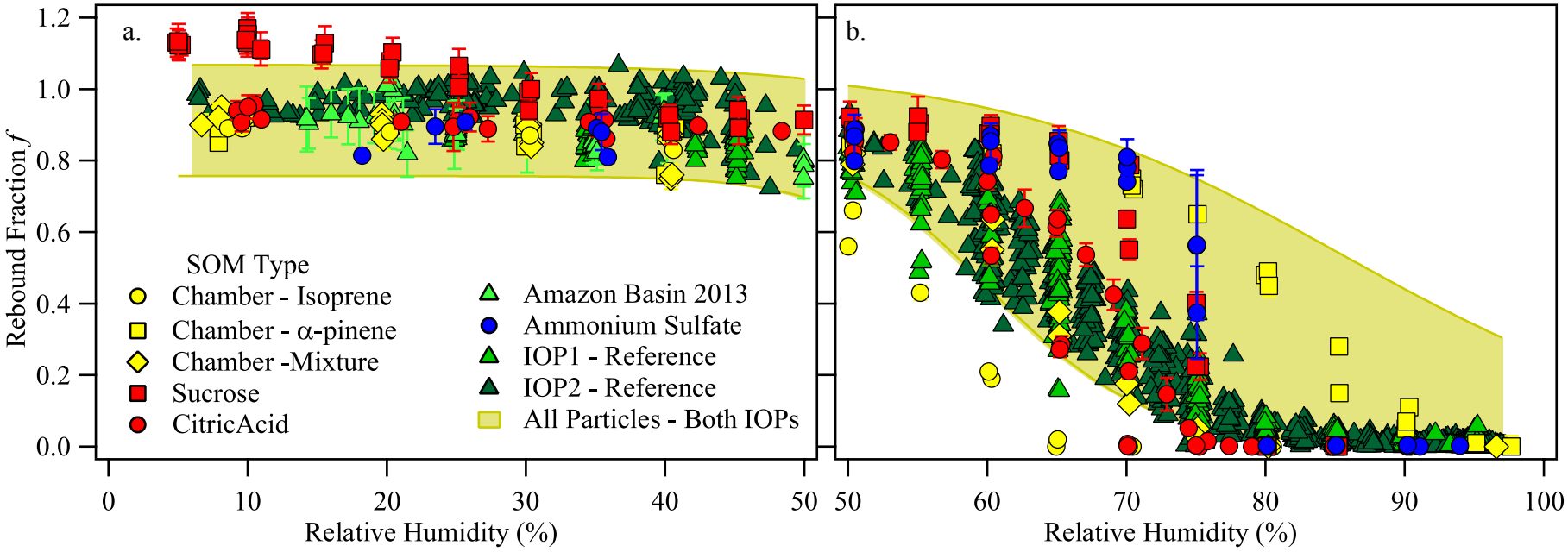
a.
b.
Rebound Fraction f
1.2
1.0
0.8
0.6
0.4
0.2
0.0
0
10
20
30
40
50
60
70
80
90
100
Relative Humidity (%)
Relative Humidity (%)
SOM Type
Chamber - Isoprene
Chamber - α-pinene
Chamber -Mixture
Sucrose
CitricAcid
Amazon Basin 2013
Ammonium Sulfate
IOP1 - Reference
IOP2 - Reference
All Particles - Both IOPs

Figure S5